ACS APPLIED MATERIALS & INTERFACES

Research Article

www.acsami.org

A Multilayered Silicon-Reduced Graphene Oxide Electrode for High Performance Lithium-Ion Batteries

Xianfeng Gao, Jianyang Li, Yuanyuan Xie, Dongsheng Guan, and Chris Yuan*

Department of Mechanical Engineering, University of Wisconsin, Milwaukee, Wisconsin 53201, United States

Supporting Information

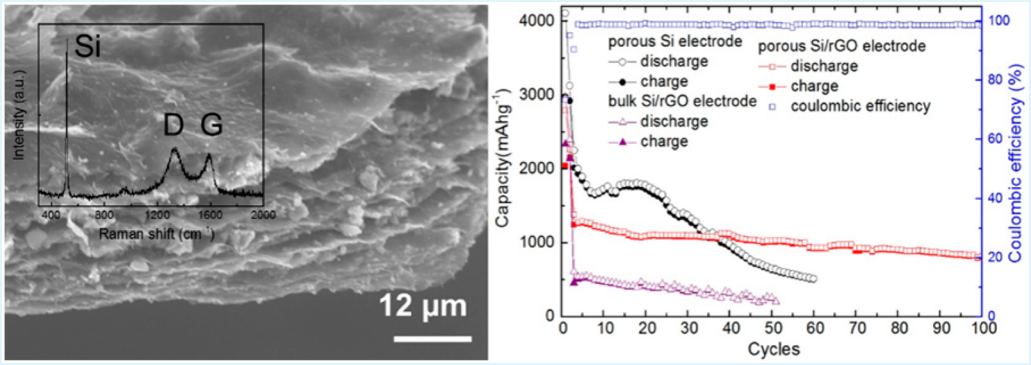

ABSTRACT: A multilayered structural silicon-reduced graphene oxide electrode with superior electrochemical performance was synthesized from bulk Si particles through inexpensive electroless etching and graphene self-encapsulating approach. The prepared composite electrode presents a stable charge−discharge performance with high rate, showing a reversible capacity of 2787 mAh g^{-1} at a charging rate of 100 mA g^{-1}, and a stable capacity over 1000 mAh g^{-1} was retained at 1 A g^{-1} after 50 cycles with a high columbic efficiency of 99% during the whole cycling process. This superior performance can be attributed to its novel multilayered structure with porous Si particles encapsulated, which can effectively accommodate the large volume change during the lithiation process and provide increased electrical conductivity. This facile low-cost approach offers a promising route to develop an optimized carbon encapsulated Si electrode for future industrial applications.

KEYWORDS: *multilayered structure, silicon−graphene electrode, lithium-ion battery, anode, low cost*

1. INTRODUCTION

Lithium-ion batteries (LIBs) have become essential energy storage devices for a rich variety of applications including portable electronics, electric vehicles, and microelectronic devices because of their high energy density, long cyclic life, and environmental compatibility.[1−3] However, current LIBs suffer from a limited storage capacity, and LIB technologies with higher capacity and energy density are needed to meet the increasing demand of industrial applications. Silicon has been identified as a promising anode material because it possesses a high theoretical capacity of 3579 mAh g^{-1} at room temperature that accommodates 3.75 Li atoms per Si atom, which is about 10 times that of the present commercial graphite anodes (372 mAh g^{-1}).[4] Unfortunately, using silicon in LIB anode has met some scientific and technical challenges in reality. Besides silicon's intrinsic electrical conductivity, another major challenge is the mechanical fracture caused by tremendous volume changes, up to 400% during the lithiation/delithiation process, leading to several severe fading mechanisms, including pulverization of the active materials, contact loss with conductive carbon agents, and unstable solid electrolyte interphase (SEI) formation.[5,6]

In the past, numerous electrode designs have emerged to circumvent this problem and improve the overall electrochemical performance of Si anodes. It was found the structure of electrode materials plays an important role in affecting the transport behavior of Li ions and the electrochemical performance of LIBs.[7] As a result, various nanostructured silicon materials such as nanoparticles,[8] nanowires,[5,9−11] Si nanotubes,[12] and nanoporous Si[13,14] have been developed and applied in LIB electrode. It demonstrated that these strucutures can partially accommodate the large volume expansion/contraction of Si anode duing the lithalization process, thus exhibiting an improved cycling performance. However, the production of nanostructured Si usually involves high-temperature pyrolysis of toxic and expensive organic silicon precursors, which may limit their practical applications.[5,13,15,16] To overcome these obstacles, it is highly desirable to develop efficient low-cost routes that can produce porous Si structure with high yield and scalable potential, which will generate

Received: October 8, 2014
Accepted: March 31, 2015
Published: March 31, 2015

ACS Publications © 2015 American Chemical Society

DOI: 10.1021/acsami.5b01230
ACS Appl. Mater. Interfaces 2015, 7, 7855−7862

meaningful impact on the actual application of Si as lithium battery anodes.

Another effective strategy for improving the Si anode performance is to use Si/C composites as stress buffering matrixes.[17−22] As a commonly used additive in lithium electrode materials, carbon coating not only enhances the electrical conductivity, but also constrains the large volume change of Si to keep the electrode integrity during the lithiation process. In this regard, composites of carbon with various morphologies of Si nanostructures, such as Si nanoparticles coated with carbon black,[17,21] Si nanoparticles in nitrogen-doped carbon sphere,[23] yolk−shell structured carbon/Si composites,[24] Si-carbon core−shell structures,[25] and graphene-coated Si nanowires,[26] have been developed to improve the electrochemcial performance of Si anodes. With the demonstrated function of bufferring the pulverization of Si upon lithiation and increasing the electric conductivity, the nanostructured Si-carbon composites have been considered as one of the most promising materials to obtain stable electrochemical performance for high capacity LIBs. Among the carbon materials, GO/graphene has been extensively used in the design of advanced Si-based anode materials[27−30] and other electrode materials,[31−33] with their superior conductivity, large specific surface area, and great flexibility. It successfully demonstrated that the reduced graphene oxide can synergistically accommodate the volume change of encapsulated electrode material and maintain their structural and electrical integrity.[34]

In this article, a new route to produce high performance Si anode from low-cost bulk Si particles was developed. Using commercial bulk Si particles, a multilayer-structured Si/reduced graphene oxide (rGO) anode was fabricated through facile electroless chemical etching, followed by the graphene self-encapsulating process governed by electrostatic interaction. Different from previously reported Si/graphene nanoparticles,[22,29,30] the obtained material is composed of micro-sized porous Si particles encapsulated in layered reduced graphene oxide, which has a low fabrication cost with inexpensive raw material and reduced amount of required graphene, but still presents excellent performance with its novel multilayered structure. In this composite, the irregular Si porous particles offer numerous void spaces that could accommodate the volume expansion of Si during lithiation, while graphene bonded to the silicon particles serves a firm and continuous electronic conduction pathway, compensating for the low electronic conductivity of intrinsic Si material. Furthermore, the overall layer-structured electrode can maintain a stable SEI layer formation during the lithiation/delithiation process. Using the silicon/graphene electrode, a reversible discharge capacity of 2787 mAh g^{-1} at a rate of 100 mA g^{-1} and 1376 mAh g^{-1} at a rate of 1 A g^{-1} with an average high columbic efficiency of ∼99% over 100 cycles has been achieved. Our approach that obtains low-cost layered structure with graphene wrapped irregular porous Si offers a new route for rational design and fabrication of scalable low-cost high-capacity stable anodes for future LIB technologies.

2. EXPERIMENTAL SECTION

Preparation of Multilayered Si−Graphene Electrode. Si powders (Sigma-Aldrich) were ultrasonicated in acetone, ethanol, and deionized water followed by boiling in a solution composed of $NH_3{\cdot}H_2O$ (30%), H_2O_2 (30%), and H_2O (1:1:5, v:v:v) for 30 min to get hydrophilic Si powders. After being rinsed with water and dried at 60 °C in a vacuum oven, the powders were added to a 50 mL solution of 37.5 mL of H_2O and 0.172 g of $AgNO_3$. 12.5 mL of HF (40%) was addd to deposit Ag catalyst on Si surface. The Ag deposition process lasts for 45 s under vigorous stirring at 30 °C. One milliliter of H_2O_2 (30%) was then added dropwise into the plating solution for metal-assisted chemical etching. The reaction was stopped after 30 min by adding a large amount of deionized water to the etching solution. The Ag particles loaded on the etched Si powders were removed by HNO_3. The etched Si powders were filtered through a micropore filter paper (0.45 μm), rinsed with deionized water, and dried at 60 °C in a vacuum oven.

Reduced graphene oxide was prepared for efficient graphene coating on the porous macro Si particles, which was prepared from commercially available aqueous graphene oxide dispersion (ACS Material). The aqueous graphene oxide was mixed with hydrazine and ammonia, followed by a 95 °C water bath for 1 h, which resulted in N doped reduced graphene oxide.[35,36] To get layered Si/rGO composite, Si powders were added into the reduced graphene oxide solution (Si:GO = 9:1, wt ratio) with ultrasonic for 5 min. Notice that ammonia was added to get a uniform graphene oxide solution during the whole process to maintain a weak alkaline environment for successful graphene coating when silicon particles were added into the solution. The resulting compound was washed with DI water, collected with micropore filter paper, and dried at 60 °C in a vacuum oven.

Coin Cell Fabrication. The Li-ion battery electrode was made by mixing the porous silicon/graphene composite with carbon black and alginate binder to form a uniform slurry in a weight ratio of 7:2:1 and then spread on a copper foil using a stainless steel blade. The electrode was dried at 60 °C in a vacuum oven for 10 h. CR2032 coin cells then were assembled in an Ar-filled glovebox using the as-prepared porous silicon/rGO anodes as working electrodes and lithium metal foil as counter electrodes. The electrolyte was 1.0 M $LiPF_6$ in ethylene carbonate/ethyl methyl carbonate (40:60, v/v) and with 1 wt % vinylene carbonate. A Celgard-2320 membrane composed of 20 μm thick polypropylene (PP)/polyethylene/PP trilayers was used as a separator.

Characterization. Hitachi S-4800 scanning electron microscopy (SEM) and Hitachi H9000NAR transmission electron microscopy (TEM) were used to characterize the morphology of the porous Si/rGO composite. The composition of the obtained material was examined by energy-dispersive X-ray spectroscopy (EDS) integrated with SEM and X-ray diffraction (XRD). The surface area and porosity of the materials were characterized by a multipoint BET N_2 adsorption/desorption method carried out on a Micromeritics ASAP 2000. Raman spectroscopy was carried out using a Renishaw 1000B Raman microscope with a 632.8 nm He−Ne laser. AC impedance over the frequency range from 100 kHz to 0.1 Hz with the amplitude of 5 mV was measured on VersaSTAT 3F (Princeton Applied Research). The charge−discharge cycles were performed between 0 and 1 V with LANHE CT2001A (Land, China).

3. RESULTS AND DISCUSSION

The synthesis of multilayered structure silicon/rGO electrode was performed through a low-cost self-encapsulating approach. Porous micro silicon particles were first obtained by metal-assisted chemical etching of commercial bulk Si particles, which are pretreated with ammonia to get a hydrophilic surface. In our experiment, $AgNO_3$ and HF are used as the source of Ag catalyst and etching agent, respectively. For multilayered Si/graphene composite synthesis, electrostatic interaction between silicon and carbon is designed to drive the self-encapsulating reaction. The surface charges of silicon and graphene are affected significantly by the pH value of the solution.[35] Graphene oxide aqueous solution was first mixed with N_2H_4 and NH_3H_2O and heated at 95 °C, which resulted in a uniform N doped reduced graphene oxide solution.[36] The pH value of the solution was adjusted to (∼7.5−8) by adding a certain amount of NH_3H_2O to get a proper environment, where

DOI: 10.1021/acsami.5b01230
ACS Appl. Mater. Interfaces 2015, 7, 7855−7862

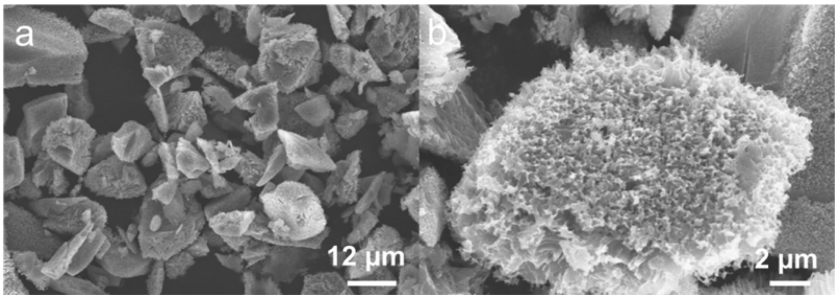

Figure 1. (a) SEM images of Si particles after electroless etching. (b) High-magnification SEM image of single Si particle shows the porous structure of etched Si.

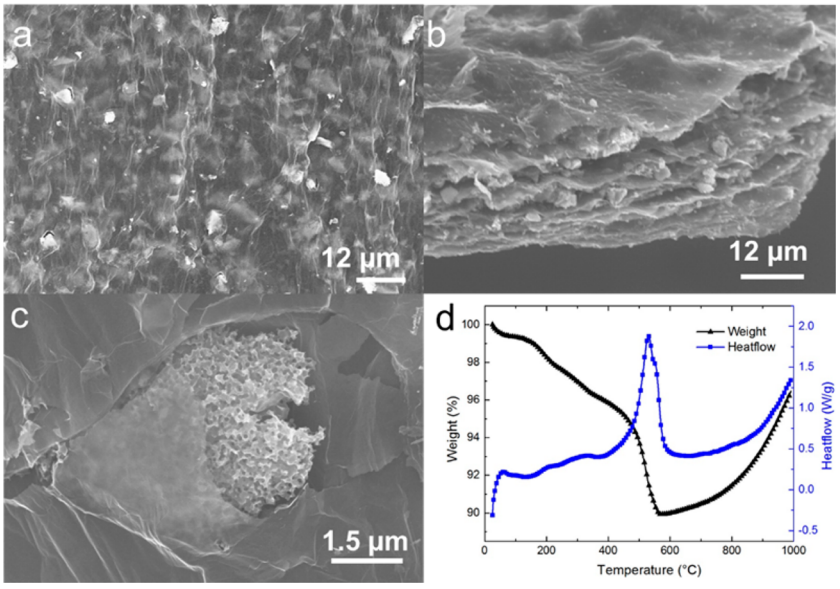

Figure 2. (a–c) SEM images of layered Si/graphene compound. (d) TGA and DSC curve of the Si/graphene composite.

opposite surface charged Si and rGO sheet could be obtained.[35] The porous silicon particles then were added into the rGO solution, which led to a spontaneous electrostatic attraction between them, forcing the Si particles to bond onto the rGO sheet. The material was finally filtered after mild stirring for 15 min. Under the combined effect of gravity and electrostatic interaction, the Si/rGO dispersed in the solution formed a multilayered structure during the filtering process, where the graphene sheet acts as a soft template. Further experimental details are provided in the Experimental Section.

Figure 1a,b presents the morphologies of the etched Si particles before combining with graphene. The etching process was not intended to change the average size of the particles (Supporting Information Figure S1), but to generate well-dispersed porous features on these particles (Figure 1). Although the obtained porous Si particles retain their irregular shapes and size variation, the generated empty spaces in the pores can partially accommodate the large volume expansion/contraction during the lithiation and delithiation process, and thus their electrochemical performance benefits. The result also confirmed that Si porous materials made by metal-assisted chemical etching have a high tolerance to the uniformity of the original bulk materials, which is important in developing low-cost industrial technologies.

Figure 2 shows the detailed characterization of the obtained multilayered structure of Si/graphene compound. Silicon is present as large micrometer-sized particles that are completely enfolded by sheets of graphene (Figure 2a). The SEM image of the edge of the multilayered composite (Figure 2b) demonstrates the layered structure of the composite, where Si particles are fully encapsulated by well-separated rGO films, which also indicates the graphene does not restack during the reduction or the following coating process. Furthermore, Si porous structure was also not damaged during the multilayer compound formation process, as shown in the high-magnification SEM images after graphene coating (Figure 2c). The tight connection between the Si particles and graphene indicates that the electrostatic interaction is an efficient way to encapsulate irregular Si micro particles into graphene sheet. It is anticipated that both the void structure of Si particles and the layered structure of Si/graphene compound would act as efficient buffer layers of the volume change, leading to superior electrochemical performance in LIB electrode. Silicon content was measured with thermogravimetric analysis (TGA) carried out in air at a heating rate of 10 °C/min (Figure 2d), giving a mass fraction of 89.9% Si. The exothermic peak centered at 530 °C observed in the differential scanning calorimetry (DSC) plot, along with a significant weight loss, corresponds to the graphene combustion reaction. After that, a gradual increase in weight and an endothermic peak in the DSC curve could be ascribed to the oxidation of Si. The relatively rapid weight increase after 600 °C indicates a fast oxidation process, which may be attributed to the porous nature of the Si particles.

DOI: 10.1021/acsami.5b01230
ACS Appl. Mater. Interfaces 2015, 7, 7855–7862

TEM was performed to investigate the detailed structure of the etched Si and porous Si/rGO composite. Figure 3a and b

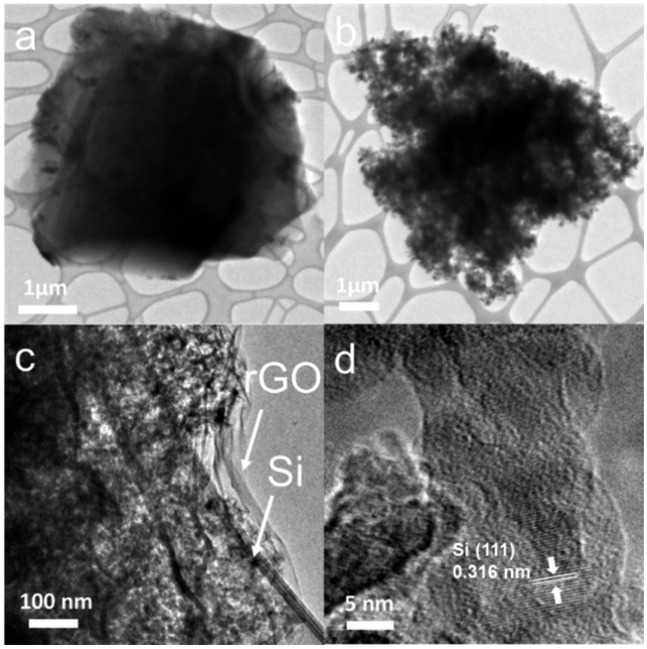

Figure 3. TEM images of (a) bulk Si particle, (b) etched porous Si particle, and (c,d) Si/rGO composite.

shows the images of single Si particle before and after chemical etching, which confirmed a porous structure obtained during the etching process. The TEM image of Si/rGO (Figure 3c) demonstrates the nature of porous Si particle encapsulated in reduced graphene oxide film. The conformal coating edge implies an intimate contact between Si and rGO. HR-TEM image (Figure 3d) indicates Si retains its crystalline structure during the whole etching and rGO coating process. The observed lattice fringes of 0.316 nm in the image (Figure 3d) correspond to the (111) plane of Si.

To verify the composition of the formed compound, energy dispersive spectroscopic (EDS) mapping of the obtained material was carried out (Figure 4). The results confirm that the bright particles in the SEM images were silicon particles with uniform graphene sheet coating. EDS mapping of the cross section of the film (Supporting Information Figure S2) also clearly indicates that silicon dispersed uniformly between rGO sheets that act as a soft template during the composite formation. From these results, we may conclude that the electrostatic-interaction-induced encapsulating process is efficient in combining porous Si micro particles with well-separated graphene sheet.

The porosities of electrode material were characterized by N_2 adsorption−desorption, as presented in Supporting Information Figure S3, and the Brunauer−Emmett−Teller (BET) surface areas of pristine bulk Si, etched porous Si, and porous Si/rGO were 1.87, 26.2, and 44.7 $m^2\ g^{-1}$, respectively. The results confirm that the chemical etching process increased the surface area of micro Si particle significantly, which make it a porous structure. The large surface areas of encapsulated porous Si electrodes are due to the intrinsic large surface areas of graphene oxide film. On the basis of the isotherms, the BJH pore size distributions were obtained (Supporting Information Figure S3b), which indicate that the metal-assisted chemical etching leads to the formation of a large amount of mesopores (2−50 nm). The BET areas and average pore sizes of three materials are summarized in Supporting Information Figure S3c. The high surface area and pore volume distribution also confirm the existence of large internal porosity available for volume expansion and larger particle−electrolyte interface, which will facilitate fast intercalation of Li^+ ions and help minimize the capacity fading due to SEI layer degradation and active material destruction.

The structure of the Si/rGO composite was further characterized by XRD and Raman spectroscopy (Figure 5). XRD patterns show the well crystalline structure of Si with characteristic peaks at 28.7°, 47.5°, 56.3°, and 69.3°, which can be assigned to the (111), (220), (311), and (400) plane of Si, respectively. The weak peak at 20.3° corresponds to the (002)

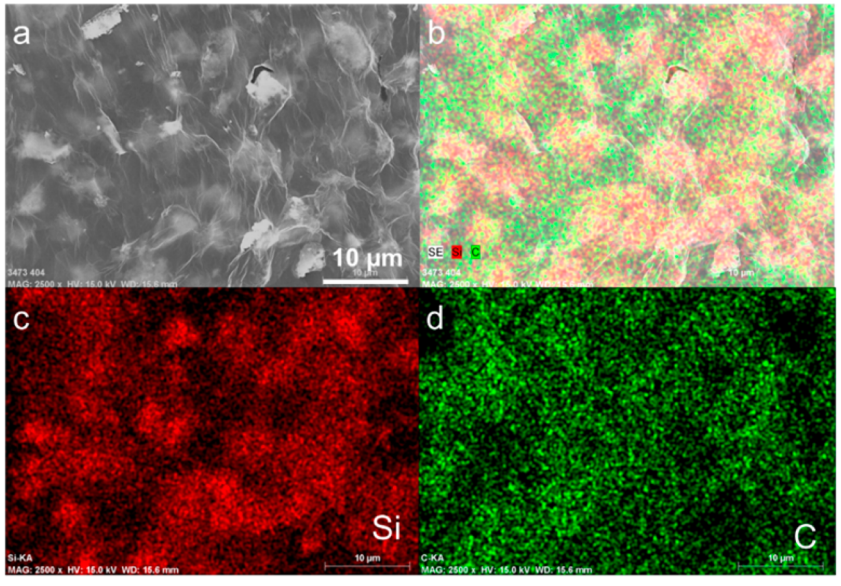

Figure 4. Elemental mapping of the Si/rGO compound. (a) SEM image of the top view of the Si/rGO compound. (b) Si and C element mapping images. (c and d) Si and C dispersion, respectively.

DOI: 10.1021/acsami.5b01230
ACS Appl. Mater. Interfaces 2015, 7, 7855−7862

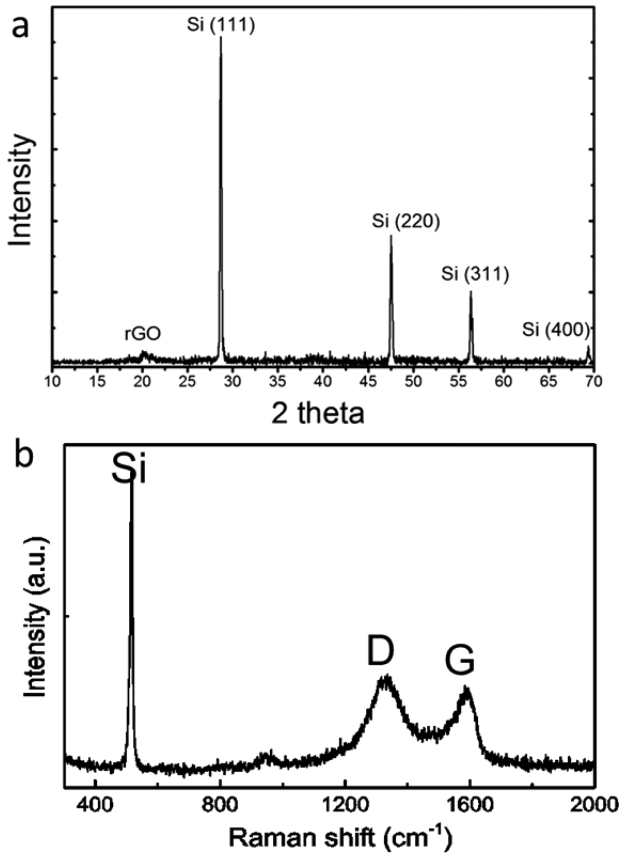

Figure 5. (a) XRD of Si/rGO composite. (b) Raman spectrum of Si/graphene composite with its characteristic silicon peak at ~520 cm^{-1}, and the D band (~1350 cm^{-1}) and G band (~1590 cm^{-1}) that are characteristic of graphene.

plane reflections of graphitic carbon. The broad diffraction peak of rGO indicates poor ordering of the sheets in the stack direction, which implies the composite was comprised mainly of single or only a few layers of rGO. The nature of the carbon and silicon in the Si/rGO composite was further analyzed by Raman spectroscopy (Figure 5b). Raman spectrum exhibits a characteristic peak at ~520 cm^{-1}, which is attributed to Si, and the other two prominent peaks at ~1350 and ~1590 cm^{-1} are the D peak, which represents the dispersive, defect-induced vibrations, and the G peak, which is related to the vibration of sp^2 bonded carbon atoms, respectively. We found that the intensities of the D and G peaks are similar, indicating that the rGO contains a large amount of disordered sp^2 carbons,[37] which are associated with the defects that may be generated during the reduction process. On the other hand, the defects also could provide extra Li diffusion channels,[38] and help electrolytes penetrate into the rGO to react with Si particle more efficiently.

Coin cells with a metallic lithium counter electrode were used to evaluate the charge/discharge performance of the multilayered Si/rGO electrode. The specific capacity values reported in Figure 6 were calculated on the basis of the total weight of Si and rGO. The cycling performance and columbic efficiency of the Si/rGO anode were tested at a rate of 1 A g^{-1} after the initial two cycles of activation at 100 mA g^{-1} (Figure 6a). An initial discharge capacity of 2787 mAh g^{-1} at a rate of 100 mA g^{-1} is obtained. When the current density is increased to 1 A g^{-1}, the Si/rGO electrode delivered a high capacity of 1376 and 1243 mAh g^{-1} for the discharge (lithiation) and charge (delithiation), respectively. The Si/rGO electrode retains a capacity of 1026 mAh g^{-1} with approximately 75% capacity retention at the 50th cycle. Note that the columbic efficiencies obtained on these batteries are over 99% during the whole 100 cycling process at 1 A g^{-1}, which indicates a good stability of the SEI and electrode structure because rupturing and reforming the SEI will consume Li.[24] For comparison, the cycling performance of a Si porous electrode without rGO is also shown in Figure 6a. The pure Si porous electrode shows relative stable performance at the first 20 cycles thanks to its intrinsic void structure, which accommodates the large volume expansion. However, its capacity fading became much faster beyond 20 cycles, and the reversible capacity dropped over 60% at 50 cycles. As a control test to confirm the role of porous structure of etched Si for electrochemical performance, the same tests were also repeated with unetched pristine Si/rGO electrode (Figure 6). The bulk Si/rGO shows a very low capacity of 608 and 457 mAh g^{-1} at 1 A g^{-1} for discharge and charge, respectively, which even decay rapidly. The result confirmed the advantage of Si porous structure. On one hand, the porous structure provides a larger surface area and therefore a larger particle−electrolyte interface to facilitate fast intercalation of Li^+ ions into Si to improve the performance at high current density. On the other hand, the porosity can provide a large void space allowing for volume expansion during the lithiation process, which make porous Si electrode able to tolerant more stress to maintain its integrity during the lithiation/delithiation process. Overall, the remarkable superior capacity retention of novel multilayered porous Si/rGO electrode can be attributed to its unique architecture where the rGO layer offers a more stable structure preventing Si from detaching from the electrode, and both the empty space in the Si pores and that between Si and graphene partially accommodate the large volume expansion/contraction during the lithiation and delithiation process.

Figure 6b shows galvanostatic cycling at a current density of 100 mA g^{-1} with a voltage ranging from 0.01 to 1.0 V. The initial discharge (lithiation)/charge (delithiation) capacities are approximately 2787 and 2042 mAh g^{-1} at 100 mA g^{-1} rate. The columbic efficiency was therefore calculated as 73%. The irreversible capacity loss may be attributed to the solid electrolyte interphase formed at the electrode/electrolyte interface and the reaction of oxygen-containing functional groups on rGO with lithium ions.[39,40] Figure 6b also demonstrates unchanged shape of the galvanostatic profile during cycling at the rate of 1 A g^{-1}, indicating a stable electrochemical behavior of Si/rGO electrode. The rate capability of the Si/rGO up to the 2 A g^{-1} was also measured (Figure 6c). The average discharge (lithiation) capacities at these rates are 2418, 1816, 1412, 1108, and 713 mAh g^{-1}, respectively, all of which are much higher than that of graphite (372 mAh g^{-1}) used in current Li ion batteries. When the rate returned to 500 mA g^{-1}, the capacity can be recovered to 1553 mAh g^{-1}, which demonstrates a stable performance on the obtained Si/rGO composite electrode. It is also noticed that the capacity decays slightly faster when tested at lower current density, which was also observed in other Si electrode works.[19,28,35,41] This tendency was also reflected by a cycling test at 200 and 500 mA g^{-1} (Supporting Information Figure S4), whose capacity decayed faster than that tested at 1 A g^{-1} in the first several cycles. The phenomenon may be attributed to the smaller volume expansion of Si under high current density

DOI: 10.1021/acsami.5b01230
ACS Appl. Mater. Interfaces 2015, 7, 7855−7862

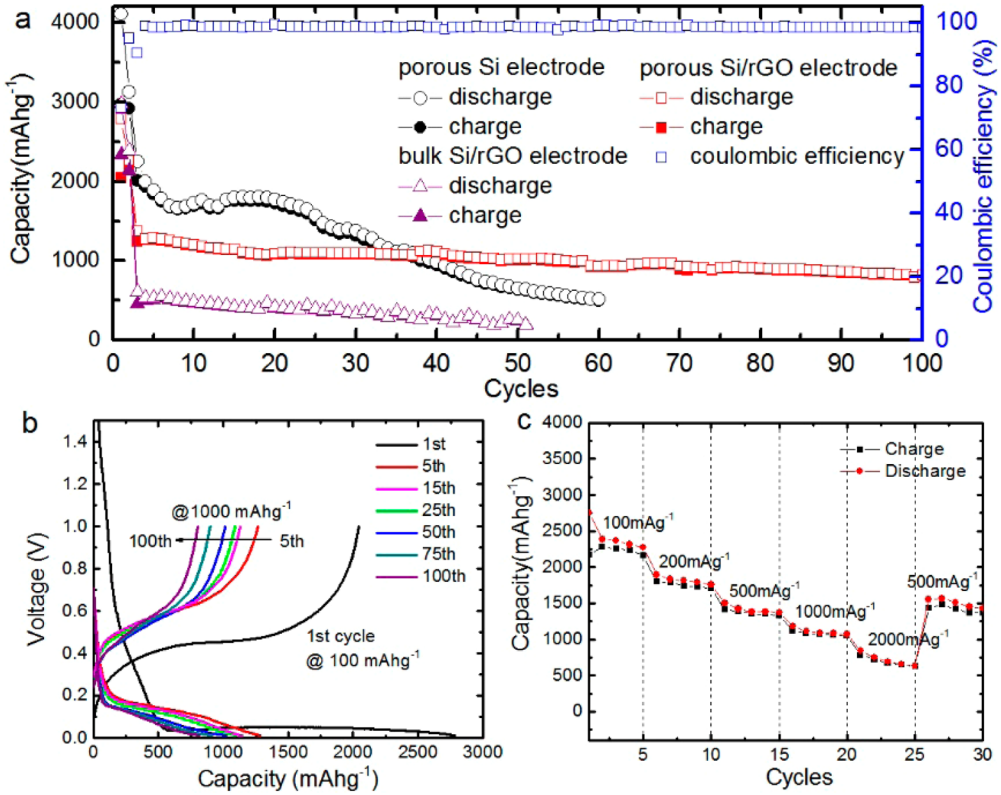

Figure 6. (a) Cycle performance at a constant current rate of 1000 mA g^{-1} after initial activation processes at 100 mA g^{-1} for two cycles; (b) galvanostatic discharge−charge profiles; and (c) rate performance of Si/graphene composite electrode.

that resulted by a relatively slower Li ion transportation rate, which will render a relatively stable SEI layer on the silicon particles that prevents the irreversible loss of lithium storage sites.[42]

To understand the reason for excellent cycling stability and rate performance, the morphology of porous Si/rGO electrodes after cycling was investigated (Supporting Information Figure S5). After 100 cycles, the morphologies of the cycled electrode were similar to that of the pristine porous Si/rGO electrode, which maintains its initial morphology and porous structure even after repeated volume changes during battery operation (Supporting Information Figure S5a−d). Such a high stability is largely due to the novel Si/rGO layered structure, where both the graphene layer and the mesopores acted as buffer layers for volume changes. The thickness of Si/rGO electrodes was also investigated by SEM before and after cycling (Supporting Information Figure S5e,f), which only shows about a 28% increase after 100 cycles. The SEM images confirmed the confinement effect of porous Si particles embedded in the graphene layers.

The superior performance can also be further understood by the electrochemical impedance spectroscopy (EIS) (Figure 7), which was tested from 100 kHz to 0.1 Hz at the charged state after 2 cycles of activation and 30 cycles of cycling. All spectra consist of a depressed semicircle attributed to the charge transfer process and a linear Warburg part attributed to the diffusion of the lithium ions in the electrode. The parameters in the model were extracted by fitting the EIS data with ZView software (Supporting Information Table S1). It is shown that the Si/rGO electrode presents significant smaller charge transfer resistance (R_{ct}, 144.7 Ω) than that of pure Si electrode (181.2 Ω) due to the superior conductivity of graphene. The

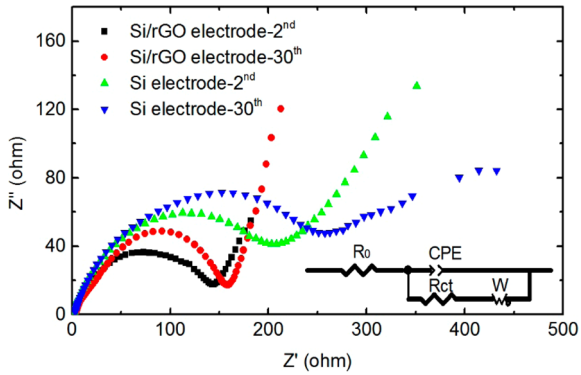

Figure 7. Impedance spectroscopy analysis of Si/rGO composite electrodes and pure porous Si electrode.

increased double layer capacitance (CPE-T, Supporting Information Table S1) and reduced diffusion resistance (W-R, Supporting Information Table S1) obtained on Si/rGO also demonstrate an enhanced Li ion diffusion activity and enlarged electrochemical active specific surface area,[43] which may be attributed to the novel multilayered Si/rGO structure and extra Li diffusion channels as induced by sp^2 defect on graphene surface. More importantly, after cycling, multilayered Si/rGO electrode presents a much smaller charge transfer resistance increase (from 144.7 to 156.2 Ω) than pure Si electrode (from 181.2 to 257.2 Ω), suggesting minor contact loss with conductive carbon agents as well as a stable SEI layer, which confirm that novel multilayered structure can effectively accommodate the volume change and enable good charge and lithium-ion transportation during the cycling process.

DOI: 10.1021/acsami.5b01230
ACS Appl. Mater. Interfaces 2015, 7, 7855−7862

4. CONCLUSION

In summary, we proposed a low-cost and scalable approach to synthesize porous Si particle-based anode for lithium-ion battery with demonstrated superior performance. The approach has enabled the preparation of a well-defined self-encapsulating layered structure of porous Si with spatially defined wrap of graphene. The enhanced reversibility and rate capability of graphene wrapped Si porous structure are attributed mainly to the void structure of Si particles and good mechanical flexibility of graphene in that it can readily accommodate the large volume change associated with lithiation/delithiation and preventing cracking of the electrode. Besides, graphene also contributes to the enhanced electronic conductivity and Li-ion diffusion activity in the electrode, which also enhances the electrochemical performance of Si/rGO electrode.

■ ASSOCIATED CONTENT

Supporting Information

SEM images of pristine Si particles, EDS mapping of Si/rGO composite at cross section, BET surface area and BJH pore size distributions analysis, cycle performance of porous Si/rGO electrode at different rates, SEM images of porous Si/rGO anodes before and after cycling, and fitted parameter of Nyquist plot. This material is available free of charge via the Internet at http://pubs.acs.org.

■ AUTHOR INFORMATION

Corresponding Author

*Tel.: (414) 229-5639. Fax: (414) 229-6958. E-mail: cyuan@uwm.edu.

Notes

The authors declare no competing financial interest.

■ ACKNOWLEDGMENTS

Financial support from the Bradley and Hertzfeld Foundations for this project is gratefully acknowledged.

■ REFERENCES

(1) Etacheri, V.; Marom, R.; Elazari, R.; Salitra, G.; Aurbach, D. Challenges in the Development of Advanced Li-ion Batteries: a Review. *Energy Environ. Sci.* **2011**, *4*, 3243−3262.

(2) Li, B.; Gao, X.; Li, J.; Yuan, C. Life Cycle Environmental Impact of High-capacity Lithium Ion Battery with Silicon Nanowires Anode for Electric Vehicles. *Environ. Sci. Technol.* **2014**, *48*, 3047−55.

(3) Goodenough, J. B.; Park, K.-S. The Li-Ion Rechargeable Battery: A Perspective. *J. Am. Chem. Soc.* **2013**, *135*, 1167−1176.

(4) Philippe, B.; Dedryvère, R.; Gorgoi, M.; Rensmo, H.; Gonbeau, D.; Edström, K. Improved Performances of Nanosilicon Electrodes Using the Salt LiFSI: A Photoelectron Spectroscopy Study. *J. Am. Chem. Soc.* **2013**, *135*, 9829−9842.

(5) Chan, C. K.; Peng, H.; Liu, G.; McIlwrath, K.; Zhang, X. F.; Huggins, R. A.; Cui, Y. High-Performance Lithium Battery Anodes Using Silicon Nanowires. *Nat. Nano* **2008**, *3*, 31−35.

(6) Teki, R.; Datta, M. K.; Krishnan, R.; Parker, T. C.; Lu, T. M.; Kumta, P. N.; Koratkar, N. Nanostructured Silicon Anodes for Lithium Ion Rechargeable Batteries. *Small* **2009**, *5*, 2236−42.

(7) Wu, H.; Cui, Y. Designing Nanostructured Si Anodes for High Energy Lithium Ion Batteries. *Nano Today* **2012**, *7*, 414−429.

(8) Kovalenko, I.; Zdyrko, B.; Magasinski, A.; Hertzberg, B.; Milicev, Z.; Burtovyy, R.; Luzinov, I.; Yushin, G. A Major Constituent of Brown Algae for Use in High-Capacity Li-Ion Batteries. *Science* **2011**, *334*, 75−79.

(9) Chockla, A. M.; Harris, J. T.; Akhavan, V. A.; Bogart, T. D.; Holmberg, V. C.; Steinhagen, C.; Mullins, C. B.; Stevenson, K. J.; Korgel, B. A. Silicon Nanowire Fabric as a Lithium Ion Battery Electrode Material. *J. Am. Chem. Soc.* **2011**, *133*, 20914−20921.

(10) Ge, M.; Rong, J.; Fang, X.; Zhou, C. Porous Doped Silicon Nanowires for Lithium Ion Battery Anode with Long Cycle Life. *Nano Lett.* **2012**, *12*, 2318−2323.

(11) Jing, S.; Jiang, H.; Hu, Y.; Li, C. Directly grown Si nanowire arrays on Cu foam with a coral-like surface for lithium-ion batteries. *Nanoscale* **2014**, *6*, 14441−14445.

(12) Park, M.-H.; Kim, M. G.; Joo, J.; Kim, K.; Kim, J.; Ahn, S.; Cui, Y.; Cho, J. Silicon Nanotube Battery Anodes. *Nano Lett.* **2009**, *9*, 3844−3847.

(13) Yao, Y.; McDowell, M. T.; Ryu, I.; Wu, H.; Liu, N.; Hu, L.; Nix, W. D.; Cui, Y. Interconnected Silicon Hollow Nanospheres for Lithium-Ion Battery Anodes with Long Cycle Life. *Nano Lett.* **2011**, *11*, 2949−2954.

(14) Zhao, Y.; Liu, X.; Li, H.; Zhai, T.; Zhou, H. Hierarchical Micro/Nano Porous Silicon Li-ion Battery Anodes. *Chem. Commun.* **2012**, *48*, 5079−5081.

(15) Chen, X.; Li, X.; Ding, F.; Xu, W.; Xiao, J.; Cao, Y.; Meduri, P.; Liu, J.; Graff, G. L.; Zhang, J.-G. Conductive Rigid Skeleton Supported Silicon as High-Performance Li-Ion Battery Anodes. *Nano Lett.* **2012**, *12*, 4124−4130.

(16) Zhong, Y.; Peng, F.; Bao, F.; Wang, S.; Ji, X.; Yang, L.; Su, Y.; Lee, S.-T.; He, Y. Large-Scale Aqueous Synthesis of Fluorescent and Biocompatible Silicon Nanoparticles and Their Use as Highly Photostable Biological Probes. *J. Am. Chem. Soc.* **2013**, *135*, 8350−8356.

(17) Magasinski, A.; Dixon, P.; Hertzberg, B.; Kvit, A.; Ayala, J.; Yushin, G. High-Performance Lithium-Ion Anodes Using a Hierarchical Bottom-Up Approach. *Nat. Mater.* **2010**, *9*, 353−358.

(18) Deng, J.; Ji, H.; Yan, C.; Zhang, J.; Si, W.; Baunack, S.; Oswald, S.; Mei, Y.; Schmidt, O. G. Naturally Rolled-Up C/Si/C Trilayer Nanomembranes as Stable Anodes for Lithium-Ion Batteries with Remarkable Cycling Performance. *Angew. Chem., Int. Ed.* **2013**, *52*, 2326−2330.

(19) Wu, H.; Zheng, G.; Liu, N.; Carney, T. J.; Yang, Y.; Cui, Y. Engineering Empty Space Between Si Nanoparticles for Lithium-Ion Battery Anodes. *Nano Lett.* **2012**, *12*, 904−9.

(20) Cui, L. F.; Hu, L.; Choi, J. W.; Cui, Y. Light-Weight Free-Standing Carbon Nanotube-Silicon Films for Anodes of Lithium Ion Batteries. *ACS Nano* **2010**, *4*, 3671−8.

(21) Jung, D. S.; Hwang, T. H.; Park, S. B.; Choi, J. W. Spray Drying Method for Large-Scale and High-Performance Silicon Negative Electrodes in Li-Ion Batteries. *Nano Lett.* **2013**, *13*, 2092−2097.

(22) Du, C.; Chen, M.; Wang, L.; Yin, G. Covalently-Functionalizing Synthesis of Si@C Core−Shell Nanocomposites as High-Capacity Anode Materials for Lithium-Ion Batteries. *J. Mater. Chem.* **2011**, *21*, 15692.

(23) Jeong, H. M.; Lee, S. Y.; Shin, W. H.; Kwon, J. H.; Shakoor, A.; Hwang, T. H.; Kim, S. Y.; Kong, B.-S.; Seo, J.-S.; Lee, Y. M.; Kang, J. K.; Choi, J. W. Silicon@porous Nitrogen-Doped Carbon Spheres through a Bottom-up Approach are Highly Robust Lithium-ion Battery Anodes. *RSC Adv.* **2012**, *2*, 4311−4317.

(24) Liu, N.; Wu, H.; McDowell, M. T.; Yao, Y.; Wang, C.; Cui, Y. A Yolk-Shell Design for Stabilized and Scalable Li-Ion Battery Alloy Anodes. *Nano Lett.* **2012**, *12*, 3315−3321.

(25) Gohier, A.; Laïk, B.; Kim, K.-H.; Maurice, J.-L.; Pereira-Ramos, J.-P.; Cojocaru, C. S.; Van, P. T. High-Rate Capability Silicon Decorated Vertically Aligned Carbon Nanotubes for Li-Ion Batteries. *Adv. Mater.* **2012**, *24*, 2592−2597.

(26) Wang, B.; Li, X.; Zhang, X.; Luo, B.; Jin, M.; Liang, M.; Dayeh, S. A.; Picraux, S. T.; Zhi, L. Adaptable Silicon−Carbon Nanocables Sandwiched between Reduced Graphene Oxide Sheets as Lithium Ion Battery Anodes. *ACS Nano* **2013**, *7*, 1437−1445.

(27) Zhou, X.; Cao, A.-M.; Wan, L.-J.; Guo, Y.-G. Spin-Coated Silicon Nanoparticle/graphene Electrode as a Binder-Free Anode for High-performance Lithium-Ion Batteries. *Nano Res.* **2012**, *5*, 845−853.

(28) Tang, H.; Tu, J.-p.; Liu, X.-y.; Zhang, Y.-j.; Huang, S.; Li, W.-z.; Wang, X.-l.; Gu, C.-d. Self-Assembly of Si/honeycomb Reduced

DOI: 10.1021/acsami.5b01230
ACS Appl. Mater. Interfaces 2015, 7, 7855−7862

Graphene Oxide Composite Film as a Binder-Free and Flexible Anode for Li-ion Batteries. *J. Mater. Chem. A* **2014**, *2*, 5834.
(29) Wu, P.; Wang, H.; Tang, Y.; Zhou, Y.; Lu, T. Three-Dimensional Interconnected Network of Graphene-Wrapped Porous Silicon Spheres: In Situ Magnesiothermic-Reduction Synthesis and Enhanced Lithium-Storage Capabilities. *ACS Appl. Mater. Interfaces* **2014**, *6*, 3546−3552.
(30) Jing, S.; Jiang, H.; Hu, Y.; Li, C. Graphene supported mesoporous single crystal silicon on Cu foam as a stable lithium-ion battery anode. *J. Mater. Chem. A* **2014**, *2*, 16360−16364.
(31) Shi, Y.; Wang, J.-Z.; Chou, S.-L.; Wexler, D.; Li, H.-J.; Ozawa, K.; Liu, H.-K.; Wu, Y.-P. Hollow Structured Li3VO4 Wrapped with Graphene Nanosheets in Situ Prepared by a One-Pot Template-Free Method as an Anode for Lithium-Ion Batteries. *Nano Lett.* **2013**, *13*, 4715−4720.
(32) Gao, X.; Li, J.; Guan, D.; Yuan, C. A Scalable Graphene Sulfur Composite Synthesis for Rechargeable Lithium Batteries with Good Capacity and Excellent Columbic Efficiency. *ACS Appl. Mater. Interfaces* **2014**, *6*, 4154−9.
(33) Yin, J.; Shi, H.; Wu, P.; Zhu, Q.; Wang, H.; Tang, Y.; Zhou, Y.; Lu, T. Graphene-Wrapped Single-crystalline Fe3O4 Nanorods with Superior Lithium-storage Capabilities. *New J. Chem.* **2014**, *38*, 4036−4040.
(34) Xu, C.; Xu, B.; Gu, Y.; Xiong, Z.; Sun, J.; Zhao, X. S. Graphene-Based Electrodes for Electrochemical Energy Storage. *Energy Environ. Sci.* **2013**, *6*, 1388−1414.
(35) Lee, W. J.; Hwang, T. H.; Hwang, J. O.; Kim, H. W.; Lim, J.; Jeong, H. Y.; Shim, J.; Han, T. H.; Kim, J. Y.; Choi, J. W.; Kim, S. O. N-doped graphitic self-encapsulation for high performance silicon anodes in lithium-ion batteries. *Energy Environ. Sci.* **2014**, *7*, 621.
(36) Li, D.; Muller, M. B.; Gilje, S.; Kaner, R. B.; Wallace, G. G. Processable Aqueous Dispersions of Graphene Nanosheets. *Nat. Nanotechnol.* **2008**, *3*, 101−5.
(37) Eckmann, A.; Felten, A.; Mishchenko, A.; Britnell, L.; Krupke, R.; Novoselov, K. S.; Casiraghi, C. Probing the Nature of Defects in Graphene by Raman Spectroscopy. *Nano Lett.* **2012**, *12*, 3925−3930.
(38) Erickson, K.; Erni, R.; Lee, Z.; Alem, N.; Gannett, W.; Zettl, A. Determination of the Local Chemical Structure of Graphene Oxide and Reduced Graphene Oxide. *Adv. Mater.* **2010**, *22*, 4467−4472.
(39) Yin, S.; Zhang, Y.; Kong, J.; Zou, C.; Li, C. M.; Lu, X.; Ma, J.; Boey, F. Y. C.; Chen, X. Assembly of Graphene Sheets into Hierarchical Structures for High-Performance Energy Storage. *ACS Nano* **2011**, *5*, 3831−3838.
(40) Hertzberg, B.; Alexeev, A.; Yushin, G. Deformations in Si−Li Anodes Upon Electrochemical Alloying in Nano-Confined Space. *J. Am. Chem. Soc.* **2010**, *132*, 8548−8549.
(41) Ge, M.; Rong, J.; Fang, X.; Zhou, C. Porous Doped Silicon Nanowires for Lithium Ion Battery Anode with Long Cycle Life. *Nano Lett.* **2012**, *12*, 2318−23.
(42) Li, B.; Yao, F.; Bae, J. J.; Chang, J.; Zamfir, M. R.; Le, D. T.; Pham, D. T.; Yue, H.; Lee, Y. H. Hollow Carbon Nanospheres/silicon/alumina Core-shell Film as an Anode for Lithium-ion Batteries. *Sci. Rep.* **2015**, *5*, 7659.
(43) Feng, Y.; Feng, N.; Wei, Y.; Bai, Y. Preparation and Improved Electrochemical Performance of SiCN−Graphene Composite Derived From Poly(silylcarbondiimide) as Li-ion Battery Anode. *J. Mater. Chem. A* **2014**, *2*, 4168.

DOI: 10.1021/acsami.5b01230
ACS Appl. Mater. Interfaces 2015, 7, 7855−7862